SAND2011-3094C

Low-Temperature Injection Dynamics and Turbulent Flame Structure in High-Pressure Supercritical Flows

Joseph C. Oefelein and Guilhem Lacaze
Sandia National Laboratories
Livermore, California 94551-0969, U.S.A.

1 Introduction

High-pressure, low-temperature combustion using liquid fuels (and/or oxidizers in the case of liquid-rockets) is a desirable mode of operation in state-of-the-art propulsion and power devices. Depending on the system, this combination has the potential to provide both high-performance and/or minimal emissions. These potential benefits are offset by a variety fundamental questions. Many of these questions center around the fact that combustion processes within the chamber are inherently turbulent, and in many cases operating pressures approach or exceed the thermodynamic critical pressure of the fuel and/or oxidizer. Operation at elevated pressures significantly increases the system Reynolds number(s) (i.e., integral-scale Reynolds numbers are of $\mathcal{O}(10^5)$ or greater), and thus inherently broadens the range of spatial and temporal turbulence scales over which interactions occur. In addition, at near-critical or supercritical conditions, thermodynamic nonidealities and transport anomalies can dominate, and there are not clear guidelines on when or how to best account for these phenomena. To address this issue, this paper focuses on the structure and dynamics of multiphase flows at high pressures. Emphasis is placed on application of Large Eddy Simulation (LES) and related subgrid-scale (SGS) models.

Research over the past decade has provided significant insights into the structure and dynamics of multiphase flows at high pressures [1–12]. Most of this research has been done in the context of liquid-rocket propulsion, which involves direct injection of both liquid fuel and/or oxidizer into the combustion chamber. However, the observed trends are equally valid for other liquid fueled devices such as Diesel engines. Depending on the pressure, injected liquid jets exhibit two distinctly different sets of evolutionary processes. At subcritical chamber pressures, the classical situation exists where a well defined interface separates the injected liquid from ambient gases due to the presence of surface tension. Dynamic shearing forces and surface tension promote primary atomization and the well known cascade of processes associated with the formation of a heterogeneous spray. Lifted spray-flames typically form as a consequence in a manner consistent with the complex exchange of mass, momentum and energy between drops and the local ambient gas mixture. The situation becomes quite different, however, as chamber pressures exceed the critical pressure of a particular propellant (i.e., liquid fuel or oxidizer). Under these conditions, a distinct gas-liquid interface does not exist. Instead, injected jets undergo a transcritical change of state as interfacial fluid temperatures rise above the critical temperature of the local mixture. Effects of surface tension become diminished, and the lack of these inter-molecular forces promote diffusion dominated mixing processes prior to atomization. The injected jets evolve in the presence of

Correspondence to: oefelei@sandia.gov

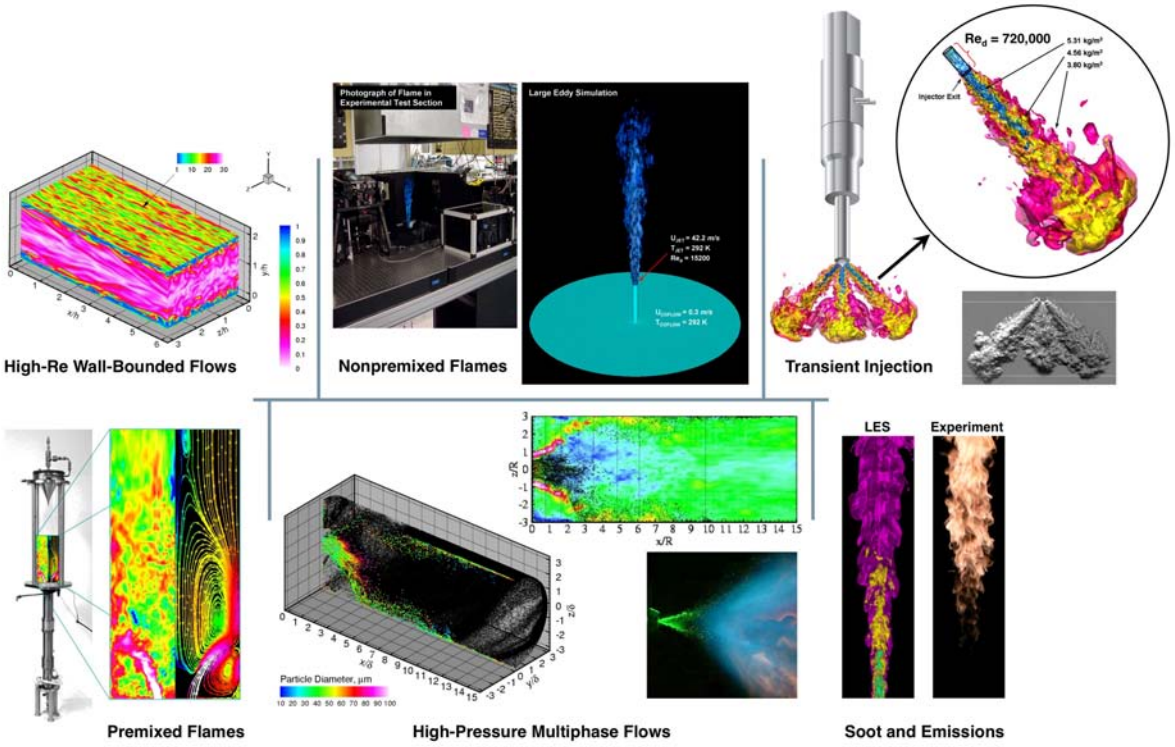

Figure 1: The RAPTOR code framework has been validated for a variety of turbulent reacting multiphase flows.

exceedingly large (but continuous) thermophysical gradients. Nonpremixed flames typically form as a consequence in the regions of high shear between the jet and ambient gas.

Modeling either of the two extremes described above numerically poses a variety of challenges. While issues related to the treatment of classical atomization and spray phenomena are well known, those related to the treatment of transcritical injection dynamics and combustion are not as well understood. This paper focuses on the latter. We begin by highlighting some of the pertinent thermophysical characteristics of high-pressure flows at application relevant conditions using two different representative flows; one relevant to liquid-rocket engines, and the other to Diesel engines. We then extend the analysis by showing recent results aimed at understanding 1) issues related to treatment of the extreme gradients in density and related variations in thermophysical properties, 2) the basic flame structure that develops as a consequence, and 3) the sensitivity of this structure to various controlling parameters such as scalar dissipation and pressure fluctuations. We perform the analysis using two configurations that provide a representative set of conditions. The first is the uni-element oxygen–hydrogen rocket experiment developed at the Pennsylvania State University, Cryogenic Combustion Laboratory, as described by Tucker *et al.* [13, 14]. The second is the baseline n-heptane experiment being studied in the high-pressure combustion vessel at Sandia National Laboratories by Pickett *et al.* [15].

2 Approach

The analysis is performed using a single unified code framework called "RAPTOR." The baseline theoretical formulation and SGS models are described by Oefelein [16]. Unlike conventional solvers, RAPTOR is a Direct Numerical Simulation (DNS) solver that has been optimized to meet the strict algorithmic requirements imposed by the LES formalism. The theoretical framework solves the fully coupled conservation equations of mass, momentum, total-energy and species for a chemically reacting

flow using multicomponent or mixture-averaged formulations. It is designed to handle high-Reynolds-number, high-pressure, real-gas and/or liquid conditions over a wide Mach operating range. It also accounts for detailed thermodynamics and transport processes at the molecular level and is sophisticated in its ability to handle a generalized SGS model framework. The model framework is capable of treating multiphase flows, sprays, and/or particulates such as soot using a Lagrangian-Eulerian formulation. The numerical formulation treats the compressible form of the conservation equations, but can be evaluated efficiently in the incompressible limit. A noteworthy aspect of RAPTOR is that it is designed specifically for LES using non-dissipative, discretely-conservative, staggered, finite-volume differencing stencils. This eliminates numerical contamination of the SGS models due to artificial dissipation and provides discrete conservation of mass, momentum, total energy and species, which is an imperative requirement for LES. The code has been optimized to provide excellent parallel scalability attributes on a wide variety of state-of-the-art computer platforms. Representative case studies are given by Oefelein *et al.* [6, 17–22]. Sample results from these studies are shown in Fig. 1.

The property evaluation scheme employed in RAPTOR is designed to account for thermodynamic non-idealities and transport anomalies over a wide range of pressures and temperatures. The scheme is comprehensive and intricate, thus only a skeletal description can be given here. The extended corresponding states model [23, 24] is employed using either Benedict-Webb-Rubin (BWR) or cubic equations of state to evaluate the *p-v-T* behavior of the inherent dense multicomponent mixtures. Use of modified BWR equations of state in conjunction with the extended corresponding states principle has been shown to provide consistently accurate results over the widest range of pressures, temperatures and mixture states, especially at near-critical conditions. A major disadvantage of the BWR equations, however, is that they are not computationally efficient. Cubic equations of state can be less accurate, especially for mixtures at near-critical or saturated conditions, but are computationally efficient. Experience has shown that both the Soave-Redlich-Kwong (SRK) and Peng-Robinson (PR) equations, when used in conjunction with the corresponding states principle, can give accurate results over the range of pressures, temperatures and mixture states typically of interest. SRK coefficients are fit to vapor pressure data and thus more suitable for conditions when reduced temperatures are less than one. PR coefficients, on the other hand, are more suitable for conditions when reduced temperatures are greater than one. A summary of the cubic equations of state and recommended constants is given by Reid *et al.* [25, Chapter 3].

Having established an analytical representation for real mixture *p-v-T* behavior, thermodynamic properties are obtained in two steps. First, respective component properties are combined at a fixed temperature using the extended corresponding states methodology outlined above to obtain the mixture state at a given reference pressure. A pressure correction is then applied using departure functions of the form given by Reid *et al.* [25, Chapter 5]. These functions are exact relations derived using Maxwell's relations (see for example VanWylen and Sonntag [26, Chapter 10]) and make full use of the real mixture *p-v-T* path dependencies dictated by the selected equation of state. Standard state properties are obtained using the databases developed by Gordon and McBride [27] and Kee *et al.* [28]. Chemical potentials and fugacity coefficients are obtained in a manner similar to that outlined above. The molecular transport properties are evaluated in a manner analogous to the thermodynamic properties. Viscosity and thermal conductivity are obtained using the extended corresponding states methodologies developed by Ely and Hanley [29, 30]. The mass diffusion coefficients and thermal diffusion coefficients are obtained using the methodologies outlined by Bird *et al.* [31] and Hirschfelder *et al.* [32] in conjunction with the corresponding states methodology proposed by Takahashi [33].

3 Results and Discussion

Using the theoretical-numerical framework described above, we have performed a select series of studies focused on the treatment of transcritical injection dynamics. The primary goal is to understand

Table 1: Key fluid properties and flow conditions associated with the uni-element oxygen–hydrogen rocket at the Pennsylvania State University and baseline n-heptane experiment being studied at Sandia National Laboratories.

	PSU Uni-Element Rocket		**Sandia Baseline n-Heptane**	
	Hydrogen	Oxygen	n-Heptane	Products[a]
Chamber Pressure, bar	70.6		43.3	
Temperature, K	295	120	373	1000
Density, kg/m^3	6.255	1110	620.7	15.28
Dynamic Viscosity, $Pa \cdot s$	8.537×10^{-6}	145.7×10^{-6}	229.2×10^{-6}	44.95×10^{-6}
Velocity, m/s	341.9	12.78	553.9	0
Mach Number	0.268	0.0223	0.772	0
Reynolds Number	$445,000$	$480,000$	$150,000$	0

[a] 0.00% O_2, 89.71% N_2, 6.52% CO_2, 3.77% H_2O

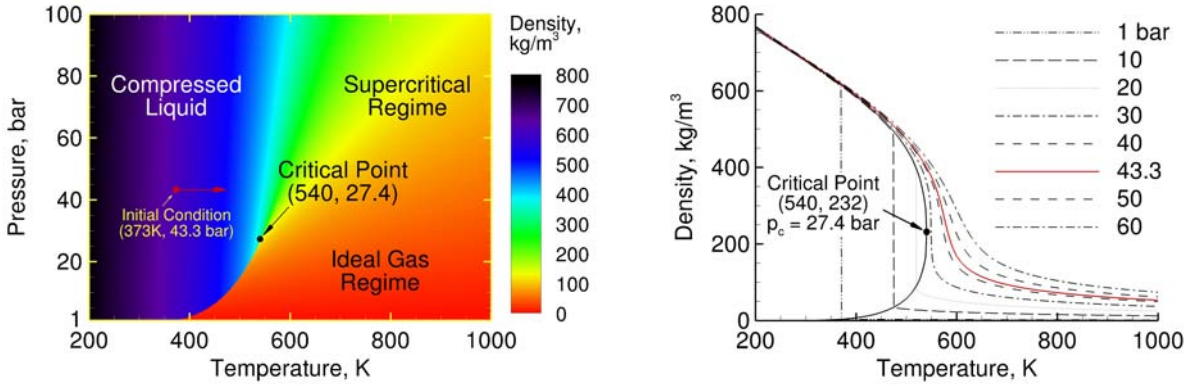

Figure 2: *p-v-T* characteristics of n-heptane showing key thermodynamic regimes and its initial state when injected into the combustion vessel. The jet enters as a compressed liquid and is heated at supercritical pressure.

basic details related to the extreme variations in density and other thermophysical properties, and how to best treat these conditions from the perspective of both modeling and numerics. To facilitate the analysis, we consider the operating conditions associated with two key target experiments. The first is the uni-element oxygen–hydrogen rocket experiment developed at the Pennsylvania State University, Cryogenic Combustion Laboratory, as described most recently by Tucker *et al.* [13, 14]. The second is the baseline n-heptane experiment being studied in the high-pressure combustion vessel at Sandia National Laboratories by Pickett *et al.* [15]. These experiments provide a representative set of operating conditions for liquid-rockets and Diesel engines, respectively. The Penn State experiment employs a single shear-coaxial injector element mounted at the head end of a chamber with a converging-diverging nozzle at the tail end. Liquid-oxygen (LOX) is injected axially through the central jet at a relatively low velocity, and gaseous-hydrogen is injected axially through the surrounding annular jet at a much higher velocity. In contrast, the Sandia experiment involves a single liquid n-heptane jet injected into a hot quiescent mixture of gaseous products where all the oxygen has been consumed to prevent the onset of combustion. Key fluid properties and flow conditions are listed in Table 1. The critical points of pure oxygen and n-heptane are ($155\ K$, $50.4\ bar$) and ($540\ K$, $27.4\ bar$), respectively. Thus, injection occurs at conditions where the LOX (in the case of the uni-element rocket) and n-heptane (in the high-pressure combustion vessel) are injected at transcritical conditions. The *p-v-T* characteristics of n-heptane showing key thermodynamic regimes and its initial state when injected into the combustion vessel is shown in Fig. 2. The LOX jet exhibits identical trends. In each case, the injected jets enter respective combustion chambers as compressed liquids and are heated at supercritical pressure.

It is well established that the transcritical nature of the injected jets described above alters the evolutionary processes that lead to the formation of a spray (e.g., Refs. [1–12]). At these conditions, interfacial

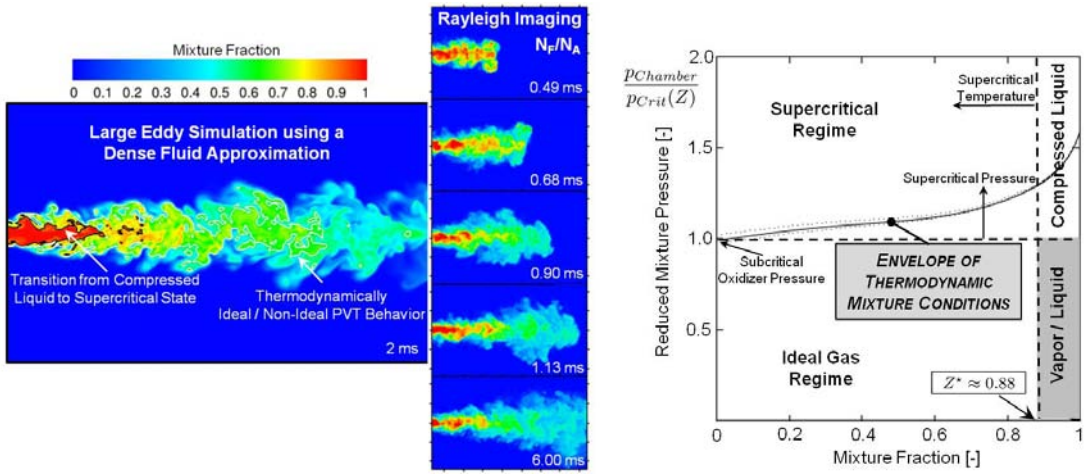

Figure 3: Qualitative comparison of the mixture fraction distribution from LES (left) and experimental Rayleigh images from the baseline n-heptane case (center). Iso-lines mark the transition from compressed liquid to supercritical mixture states (black) and the separation between regions of nonideal and ideal fluid behavior (white). The plot to the right shows the envelope of mixture states observed as a function of mixture fraction.

fluid temperatures in regions of high shear rise above the critical temperature of the local mixture. The effects of surface tension become diminished, and the lack of inter-molecular forces promote diffusion dominated mixing processes prior to atomization. Thus, issues related to modeling shift from the treatment of classical spray phenomena and the related dynamically evolving interfaces that are dominated by surface tension, to treatment of a dense nonideal fluid that exhibits extreme but continuous variations in density and the related thermophysical mixture properties. The extreme nature of these gradients poses an equally daunting set of issues related to modeling and numerical accuracy, especially for LES. To understand these issues better, we have performed a variety of calculations relevant to the two experimental target cases listed in Table 1 and will use select results to illustrate key findings.

Figure 3 shows a representative LES result for the n-heptane case. The calculation was performed using the RAPTOR code framework and dense fluid model summarized in the last section. The image to the left shows the instantaneous mixture fraction distribution predicted by LES at 2 ms after the start of injection. Iso-lines mark the transition from compressed liquid to supercritical mixture states (black), and the separation between regions of nonideal and ideal fluid behavior (white). In the center are a set of experimental Rayleigh images that provide evidence that the LES is qualitatively similar. The plot to the right shows the envelope of mixture states observed as a function of mixture fraction. This plot was obtained by mapping the temperature distribution predicted by LES to mixture fraction space, then using the related conditional averages to plot the reduced mixture critical pressure (defined as $p_{\text{Chamber}}/p_c(Z)$) as a function of mixture fraction. For this case $Z = 1$ is pure n-heptane and $Z = 0$ is the ambient product mixture listed in Table 1. This plot verifies that (for this particular case) assumptions related to the dense fluid approximation are valid for all mixture states in the domain. The constant chamber pressure of 43.3 bar exceeds the mixture critical pressure everywhere except for states close to $Z = 0$. Regions where $Z = 0$, however, are all in the ideal gas regime.

A key issue in applying the dense fluid approximation to these flows revolves around treatment of the steep but continuous gradients that develop as the jet boundary transitions from a compressed liquid to supercritical mixture states. This region is highlighted by the black isoline in Fig. 3. The combination of steep density gradients and strong differential diffusion can impose significant numerical instabilities, mass conservation errors, and flame structure anomalies. To investigate these issues using the exact same theoretical-numerical framework (i.e., RAPTOR), we have adopted the opposed-jet configuration shown in Fig. 4. In the present context, the characteristic timescales of chemistry are much smaller than

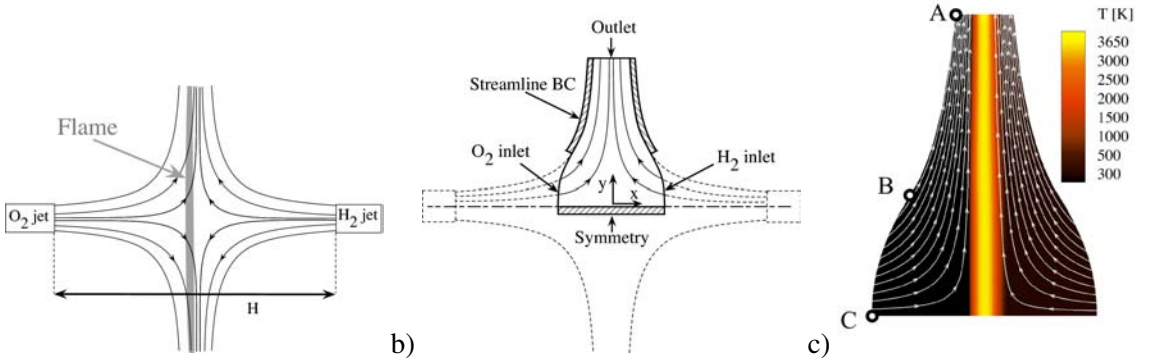

a) b) c)

Figure 4: Two-dimensional counterflow flame where a) is the theoretical configuration with H denoting the distance between inlets, b) is the computational domain, and c) a representative flow and temperature field.

turbulence and pressure oscillations and the steady flamelet assumption applies. Thus, two-dimensional steady laminar opposed-jet calculations are a valid method to study flame structure and related issues associated with various scalar gradients. For these studies, we focus on the LOX–hydrogen system listed in Table 1. This provides simplicity in terms of chemical kinetics while maintaining the desired complexities with respect to thermodynamics and transport.

Figure 4a shows a diagram of the theoretical configuration, where a laminar oxygen jet interacts with an opposed laminar hydrogen jet. A nonpremixed flame is stabilized near the stagnation point, and the applied strain mimics the effect of a turbulent eddy forcing the flow toward the flame. The shape of the numerical domain is defined using potential flow theory. Based on this theory, equations for the streamlines can be determined and the boundaries of the domain are selected to follow these paths using the computational domain shown in Fig. 4b. The boundary conditions are also imposed using potential flow theory, which allows great flexibility to modify the strain-rate and the thermodynamic conditions. The special shape of the computational domain allows one to obtain a high quality mesh with smooth and well controlled stretching. The position of point A in Fig. 4c is arbitrary. Point B is on the stream line that passes through point A and only its y-coordinate is arbitrary. Between points B and C, a second order polynomial function is used to get a normal tangent at $y = 0$, and an inflection point at B. This facilitates the generation of high-quality near-orthogonal stretched grid topologies.

As an example of the types of studies performed, we show recent results that focus on flame structure and nonideal real-fluid effects. Five different cases have been considered. The first is aimed at validating our present approach against the DNS of Ribert *et al*. [9]. Cases 2–4 focus on the effects of strain, pressure and temperature on the flame structure. Case 5 investigates real-fluid effects on the flame. For this case, the temperature of oxygen is set to $154\ K$, which is slightly lower that the critical temperature. By varying the pressure a few bars around the critical pressure, it is possible to obtain transcritical oxygen or gaseous oxygen in a manner that isolates differences in the flame structure to thermodynamic nonidealties. Because of space limitations, only the main conclusions of Cases 1 through 4 are presented to allow a more detailed analysis of the real-fluid effects observed with respect to Case 5.

The strain-rate employed for the reference calculations of Ribert *et al*. (Case 1) was $a = 2000\ s^{-1}$, at $50\ bar$. Oxygen and hydrogen are injected at supercritical temperatures of $300\ K$. Good agreement was obtained between the the present approach and these reference calculations. Thus, it was concluded that the opposed-jet configuration shown in Fig 4 coupled with the RAPTOR code framework can be used to accurately study flame structure and related phenomena at high-pressure. Subsequent cases were performed at conditions similar to those listed in Table 1 using a maximum strain-rate of approximately $a = 10^6\ s^{-1}$. To investigate the effects on flame structure, the strain-rate was varied from $5 \times 10^4\ s^{-1}$ to $5 \times 10^6\ s^{-1}$. The flame was found to be robust over this range, which indicates that the maximum

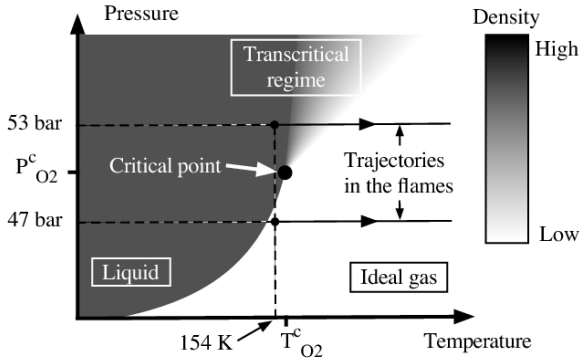

Figure 5: Pressures and heating trajectories used to study the impact of real-fluid phenomena on flame structure.

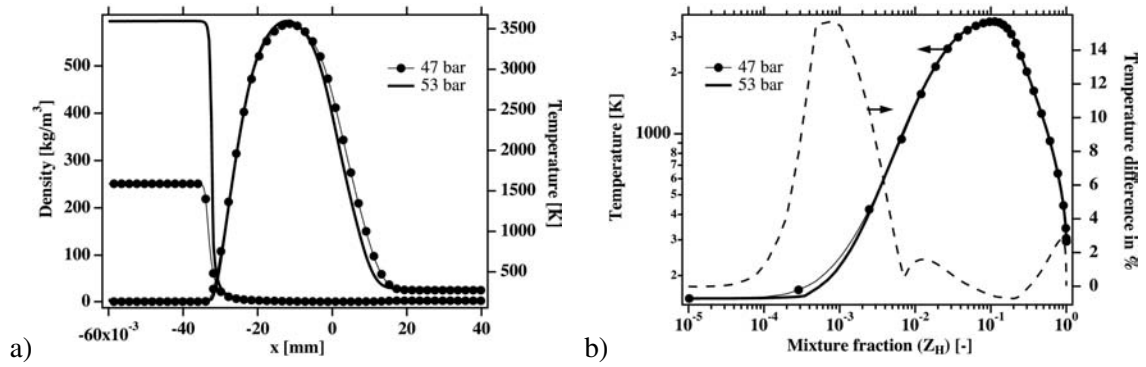

Figure 6: Effects of real-fluid nonidealities on a) the temperature and density distributions in physical space, and b) the temperature distribution in mixture fraction space for $T_{O_2} = 154\ K$, $T_{H_2} = 295\ K$, and $a = 10^5\ s^{-1}$.

temperature is insensitive to any variation of strain up to $a = 5 \times 10^6\ s^{-1}$. At this magnitude, the maximum temperature decreases slightly due to the fact that the chemical and mixing timescales become comparable. In the range of interest, the flame is thin and its structure in mixture fraction space is not affected by strain, which indicates that the flamelet assumption is valid. We have also shown that the reaction zone thickness in physical space follows the asymptotic relation $\delta_{\text{flame}} \propto 1/\sqrt{a}$.

Pressure effects are investigated over the range 53 to $90\ bar$. This range was selected to study the effect of pressure oscillations that approach 30% of the mean pressure in a rocket engine operated at $70\ bar$. In mixture fraction space, quantities in the flame front are not impacted by pressure variations. In physical space, the reaction layer (which is a governed by species diffusion) is sensitive to pressure as $\delta_{\text{flame}} \propto 1/\sqrt{P}$. Outside the reaction zone, transport and thermodynamic properties are significantly affected by pressure variations, especially in the region where the dense oxygen heats up. This last observation is a direct consequence of highly nonlinear real-fluid phenomena. To investigate the impact of real-fluid phenomena as a function of pressure, inlet temperatures were fixed and thermodynamic conditions were varied by changing the pressure. In the present study, the inlet temperature of oxygen is set to $154\ K$ (one Kelvin below the critical temperature) and the injection temperature of hydrogen is set to $295\ K$. One flame is studied at $47\ bar$, where the oxygen does not experience transcritical effects. A second flame is studied at $53\ bar$ in the transcritical regime. The reference pressures and heating trajectories used for these two flames on a pressure-temperature diagram for oxygen are shown in Fig. 5.

The temperature and density of the two flames at the conditions described above are shown in Fig. 6. In physical space (Fig. 6a), the temperature profile across the $53\ bar$ flame is slightly narrower than the flame at $47\ bar$. This is mainly due to the effect of pressure on the flame thickness. The maximum temperature of the two flames are the same and the main difference is observed in the density profiles.

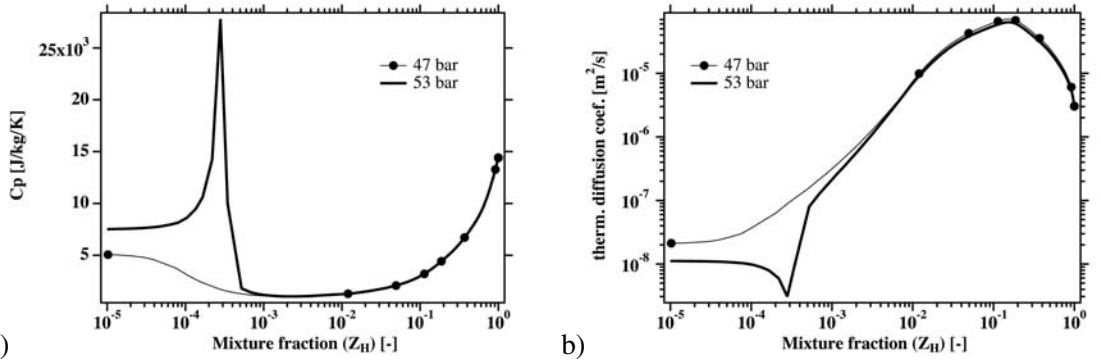

Figure 7: Effects of real-fluid thermodynamics and transport in mixture fraction space on a) the heat capacity of the mixture (C_p), and b) thermal diffusion coefficient (D_{th}) for $T_{O_2} = 154\ K$, $T_{H_2} = 295\ K$, and $a = 10^5\ s^{-1}$.

For the flame at $53\ bar$, the injection density of the oxygen is $587\ kg/m^3$, whereas the flame at $47\ bar$ is fed with a $245\ kg/m^3$ stream. Figure 6b shows the temperature distribution across the two flames in mixture fraction space. For clarity, the temperature difference is indicated in percent. Nonideal real-fluid effects are observed for mixture fraction values of $Z \approx 10^{-3}$, where the difference between the two temperature curves is about 15%. This indicates that near the critical point, a variation of 11% of the pressure induces a 15% variation of the temperature, and for high-pressure combustion the chemistry must be handled with a code that can accommodate nonideal real-fluid phenomena. No significant real-fluid effects effects were observed for the species distributions and thus they are not shown.

Real-fluid effects are further investigated by focusing on the thermodynamic and transport properties. Figure 7 shows a) the heat capacity at constant pressure, and b) the thermal diffusion coefficient across the two flames. Significant differences can be observed for these quantities at higher pressures in the low temperature regions. The heat capacity in the transcritical flame at $53\ bar$ exhibits a strong peak in the vicinity of the steep density gradient. In contrast, the lower pressure flame at $47\ bar$ does not exhibit such phenomenon. Similar observations can be made with respect to the thermal diffusion coefficients across the flames. This thermal barrier is the cause of the difference shown in the temperature profiles in Fig. 6b. The collection of results from all the cases suggests that, in the flame zone, temperature and species profiles in mixture fraction space are insensitive to strain, pressure, and inlet temperatures. In nonreacting areas, pressure and injection temperatures can have a significant impact on thermodynamic and transport properties, and to some degree also on temperature.

4 Conclusions

Pertinent thermophysical characteristics of high-pressure flows, where one of the working fluids is injected in a state that is subcritical with respect to temperature and supercritical with respect to pressure have been outlined. Two sets of application relevant conditions were used as representative systems; one relevant to liquid-rocket engines using hydrogen and oxygen, and the other to Diesel engines using n-heptane and hot combustion products. Primary emphasis was placed on 1) issues related to treatment of the extreme gradients in density and related variations in thermophysical properties, 2) the basic flame structure that develops as a consequence, and 3) the sensitivity of this structure to various controlling parameters such as scalar dissipation and pressure fluctuations. The analysis was performed using a single unified theoretical-numerical framework. Using this framework, a select series of studies were performed that focused transcritical injection dynamics. The primary goal is to understand basic details related to the extreme variations in density and other thermophysical properties, and how to best treat these conditions from the perspective of both modeling and numerics.

Results using n-heptane injected into a high-pressure combustion vessel of hot products illustrated key instantaneous mixing characteristics that exist when fuel is injected at high-pressure supercritical conditions. Iso-lines mark the transition from compressed liquid to supercritical mixture states and the separation between regions of nonideal and ideal fluid behavior. The envelope of mixture states observed as a function of mixture fraction were also mapped to show that (for the particular set of conditions selected here) the assumptions related to the dense fluid approximation were valid. A key issue highlighted in applying the dense fluid approximation revolves around treatment of the steep but continuous gradients that develop as the jet boundary transitions from a compressed liquid to supercritical mixture states. The combination of steep density gradients and strong differential diffusion can induce significant numerical instabilities, mass conservation errors, and flame structure anomalies.

To investigate flame structure anomalies, an opposed-jet configuration was adopted. For these studies, we focused on oxygen–hydrogen systems to provide simplicity in terms of chemical kinetics while maintaining the desired complexities with respect to thermodynamics and transport. Results from several cases were summarized. Analysis revealed that steady laminar counterflow flames are appropriate to study the flame structure. The solver was shown to correctly capture the flame structure at high-pressure and high strain-rates. The collection of results suggests that in the flame zone, temperature and species profiles in mixture fraction space are insensitive to strain, pressure, and inlet temperatures. In nonreacting areas, however, pressure and injection temperatures can have a significant impact on thermodynamic and transport properties, and to some degree also on flame temperature. Results also demonstrated the effect of real-fluid phenomena on the flame structure. At conditions close to the critical point of oxygen, small pressure variations were imposed to alter the heating trajectory of the flame such that the flow transitioned from a transcritical regime to a near ideal gas regime. These modifications had a significant impact on the thermodynamic and transport processes and the flow temperature in the vicinity of the steep density gradient. This indicates that real-fluid effects must to be taken into account in companion combustion models to correctly represent mixing processes and their interaction with the flame.

References

[1] M. Oschwald, J. Smith, R. Branam, J. Hussong, A. Schik, B. Chehroudi, and D. Talley. Injection of fluids into supercritical environments. *Combustion Science and Technology*, 178(1-3):49–100, 2006.

[2] M. Habiballah, M. Orain, F. Grisch, L. Vingert, and P. Gicquel. Experimental studies of high-pressure cryogenic flames on the mascotte facility. *Combustion Science and Technology*, 178(1-3):101–128, 2006.

[3] K.-C. Lin, S. Cox-Stouffer, and T. Jackson. Structures and phase transition processes of supercritical methane/ethylene mixtures injected into a subcritical environment. *Combustion Science and Technology*, 178(1-3):129–160, 2006.

[4] S. Candel, M. Juniper, G. Singla, P. Scouflaire, and C. Rolon. Structure and dynamics of cryogenic flames at supercritical pressure. *Combustion Science and Technology*, 178(1-3):161–192, 2006.

[5] N. Zong and V. Yang. Cryogenic fluid jets and mixing layers in transcritical and supercritcal environments. *Combustion Science and Technology*, 178(1-3):193–228, 2006.

[6] J. C. Oefelein. Mixing and combustion of cryogenic oxygen-hydrogen shear-coaxial jet flames at supercritical pressure. *Combustion Science and Technology*, 178(1-3):229–252, 2006.

[7] J. Bellan. Theory, modeling and analysis of turbulent supercritical mixing. *Combustion Science and Technology*, 178(1-3):253–281, 2006.

[8] L. C. Selle, N. A. Okong'o, J. Bellan, and K. G. Harstad. Modelling of subgrid-scale phenomena in supercritical transitional mixing layers: An a priori study. *Journal of Fluid Mechanics*, 593:57–91, 2007.

[9] G. Ribert, N. Zong, V. Yang, L. Pons, N. Darabiha, and S. Candel. Counterflow diffusion flames of general fluids: Oxygen/hydrogen mixtures. *Combustion and Flame*, 154:319–330, 2008.

[10] G. Lacaze, B. Cuenot, T. Poinsot, and M. Oschwald. Large eddy simulation of laser ignition and compressible reacting flow in a rocket-like configuration. *Combustion and Flame*, 156:1166–1180, 2009.

[11] L. Pons, N. Darabiha, S. Candel, G. Ribert, and V. Yang. Mass transfer and combustion in transcritical nonpremixed counterflows. *Combustion Theory and Modelling*, 13:57–81, 2009.

[12] T. Schmitt, Y. Méry, M. Boileau, and S. Candel. Large-eddy simulation of oxygen/methane flames under transcritical conditions. *Proceedings of the Combustion Institute*, 33:1383–1390, 2011.

[13] P. K. Tucker, S. Menon, C. L. Merkle, J. C. Oefelein, and V. Yang. An approach to improved credibility of CFD simulations for rocket injector design. *43rd AIAA/ASME/SAE/ASEE Joint Propulsion Conference and Exhibit, Paper 2007-5572*, July 8-11 2007. Cincinnati, Ohio.

[14] P. K. Tucker, S. Menon, C. L. Merkle, J. C. Oefelein, and V. Yang. Validation of high-fidelity CFD simulations for rocket injector design. *44th AIAA/ASME/SAE/ASEE Joint Propulsion Conference and Exhibit, Paper 2008-5526*, July 21-23 2008. Hartford, Connecticut.

[15] L. M. Pickett. Engine combustion network. www.ca.sandia.gov/ECN, 2005-2011. Combustion Research Facility, Sandia National Laboratories.

[16] J. C. Oefelein. Large eddy simulation of turbulent combustion processes in propulsion and power systems. *Progress in Aerospace Sciences*, 42(1):2–37, 2006.

[17] J. C. Oefelein. Thermophysical characteristics of LOX–H_2 flames at supercritical pressure. *Proceedings of the Combustion Institute*, 30:2929–2937, 2005.

[18] J. C. Oefelein, R. W. Schefer, and R. W. Barlow. Toward validation of LES for turbulent combustion. *AIAA Journal*, 44(3):418–433, 2006.

[19] J. C. Oefelein, V. Sankaran, and T. G. Drozda. Large eddy simulation of swirling particle-laden flow in a model axisymmetric combustor. *Proceedings of the Combustion Institute*, 31:2291–2299, 2007.

[20] V. Sankaran, T. G. Drozda, and J. C. Oefelein. A tabulated closure for turbulent nonpremixed combustion based on the linear eddy model. *Proceedings of the Combustion Institute*, 32:1571–1578, 2009.

[21] J. H. Frank, S. A. Kaiser, and J. C. Oefelein. Analysis of scalar mixing dynamics in LES using high-resolution imaging of laser Rayleigh scattering in turbulent non-reacting jets and non-premixed jet flames. *Proceedings of the Combustion Institute*, 33:1373–1381, 2011.

[22] A. M. Kempf, B. J. Geurts, and J. C. Oefelein. Error analysis of large eddy simulation of the turbulent non-premixed Sydney bluff-body flame. *Combustion and Flame*, 2011. Accepted.

[23] T. W. Leland and P. S. Chappelear. The corresponding states principle. A review of current theory and practice. *Industrial and Engineering Chemistry Fundamentals*, 60(7):15–43, 1968.

[24] J. S. Rowlinson and I. D. Watson. The prediction of the thermodynamic properties of fluids and fluid mixtures–I. The principle of corresponding states and its extensions. *Chemical Engineering Science*, 24(8): 1565–1574, 1969.

[25] R. C. Reid, J. M. Prausnitz, and B. E. Polling. *The Properties of Liquids and Gases*. McGraw-Hill, New York, New York, 4th edition, 1987.

[26] G. J. VanWylen and R. E. Sonntag. *Fundamentals of Classical Thermodynamics*. John Wiley and Sons, Incorporated, New York, New York, 3rd edition, 1986.

[27] S. Gordon and B. J. McBride. Computer program for calculation of complex chemical equilibrium compositions, rocket performance, incident and reflected shocks and Chapman-Jouguet detonations. Technical Report NASA SP-273, National Aeronautics and Space Administration, 1971.

[28] R. J. Kee, F. M. Rupley, and J. A. Miller. Chemkin thermodynamic data base. Technical Report SAND87-8215B, Sandia National Laboratories, 1990. Supersedes SAND87-8215 dated April 1987.

[29] J. F. Ely and H. J. M. Hanley. Prediction of transport properties. 1. Viscosity of fluids and mixtures. *Industrial and Engineering Chemistry Fundamentals*, 20(4):323–332, 1981.

[30] J. F. Ely and H. J. M. Hanley. Prediction of transport properties. 2. Thermal conductivity of pure fluids and mixtures. *Industrial and Engineering Chemistry Fundamentals*, 22(1):90–97, 1981.

[31] R. B. Bird, W. E. Stewart, and E. N. Lightfoot. *Transport Phenomena*. John Wiley and Sons, Incorporated, New York, New York, 1960.

[32] J. O. Hirschfelder, C. F. Curtiss, and R. B. Bird. *Molecular Theory of Gases and Liquids*. John Wiley and Sons, Incorporated, New York, New York, 2nd edition, 1964.

[33] S. Takahashi. Preparation of a generalized chart for the diffusion coefficients of gases at high pressures. *Journal of Chemical Engineering of Japan*, 7(6):417–420, 1974.